

AD

TECHNICAL REPORT ARCCB-TR-97005

**THERMOCHEMICAL EROSION MODELING
OF ORIGINAL M242/M919 GUN SYSTEM**

SAMUEL SOPOK
GEORGE PFLEGL
PETER O'HARA
STUART DUNN
DOUGLAS COATS

FEBRUARY 1997



**US ARMY ARMAMENT RESEARCH,
DEVELOPMENT AND ENGINEERING CENTER
CLOSE COMBAT ARMAMENTS CENTER
BENÉT LABORATORIES
WATERVLIET, N.Y. 12189-4050**



APPROVED FOR PUBLIC RELEASE; DISTRIBUTION UNLIMITED

DTIC QUALITY INSPECTED 8

19970425 063

DISCLAIMER

The findings in this report are not to be construed as an official Department of the Army position unless so designated by other authorized documents.

The use of trade name(s) and/or manufacturer(s) does not constitute an official endorsement or approval.

DESTRUCTION NOTICE

For classified documents, follow the procedures in DoD 5200.22-M, Industrial Security Manual, Section II-19 or DoD 5200.1-R, Information Security Program Regulation, Chapter IX.

For unclassified, limited documents, destroy by any method that will prevent disclosure of contents or reconstruction of the document.

For unclassified, unlimited documents, destroy when the report is no longer needed. Do not return it to the originator.

REPORT DOCUMENTATION PAGE

Form Approved
OMB No. 0704-0186

Public reporting burden for this collection of information is estimated to average 1 hour per response, including the time for reviewing instructions, searching existing data sources, gathering and maintaining the data needed, and completing and reviewing the collection of information. Send comments regarding this burden estimate or any other aspect of this collection of information, including suggestions for reducing this burden, to Washington Headquarters Services, Directorate for Information Operations and Reports, 1215 Jefferson Davis Highway, Suite 1204, Arlington, VA 22202-4302, and to the Office of Management and Budget, Paperwork Reduction Project (0704-0186), Washington, DC 20503.

1. AGENCY USE ONLY (Leave blank)	2. REPORT DATE	3. REPORT TYPE AND DATES COVERED	
	February 1997	Final	
4. TITLE AND SUBTITLE THERMOCHEMICAL EROSION MODELING OF ORIGINAL M242/M919 GUN SYSTEM		5. FUNDING NUMBERS AMCMS No. 6226,24,H180.0 PRON No. 4A6B6FYK1ABJ	
6. AUTHOR(S) Samuel Sopok, George Pflegl, Peter O'Hara, Stuart Dunn*, and Douglas Coats* * Software and Engineering Associates, Inc., Carson City, NV		8. PERFORMING ORGANIZATION REPORT NUMBER ARCCB-TR-97005	
7. PERFORMING ORGANIZATION NAME(S) AND ADDRESS(ES) U.S. Army ARDEC Benet Laboratories, AMSTA-AR-CCB-O Watervliet, NY 12189-4050			
9. SPONSORING/MONITORING AGENCY NAME(S) AND ADDRESS(ES) U.S. Army ARDEC Close Combat Armaments Center Picatinny Arsenal, NJ 07806-5000		10. SPONSORING/MONITORING AGENCY REPORT NUMBER	
11. SUPPLEMENTARY NOTES Presented at the 1996 JANNAF 33rd Combustion Meeting, Monterey, CA, 4-8 November 1996. Published in proceedings of the meeting.			
12a. DISTRIBUTION/AVAILABILITY STATEMENT Approved for public release; distribution unlimited.		12b. DISTRIBUTION CODE	
13. ABSTRACT (Maximum 200 words) The MACE gun barrel thermochemical erosion modeling code addresses wall degradations due to transformations, chemical reactions, and cracking coupled with pure mechanical erosion for the original M242/M919 gun system. This predictive tool provides gun system design information that is otherwise impractical. The A723, 0.002-inch plated chromium/A723, and 0.002-inch sputtered tantalum/A723 wall materials are evaluated for erosion using the M242 Cycle A firing scenario. This complex computer analysis is based on rigorously evaluated scientific theory that has been validated in the rocket community over the last forty years. Our gun erosion analysis includes the standard interior ballistics gun code (XNOVAKTC), the standard nonideal gas-wall thermochemical rocket code modified for guns (CCET), the standard mass addition boundary layer rocket code modified for guns (MABL), and the standard wall material ablation conduction erosion rocket code modified for guns (MACE). This analysis provides wall material erosion predictions and comparisons (ablation, conduction, and erosion profiles) as a function of time, travel (customer-selected 6-inch, 12-inch, 30-inch), and number of rounds to barrel condemnation. These original M242/M919 gun system predictions agree well with the standard wall heat transfer/temperature profile code (FDHEAT) and actual measured gun system erosion data.			
14. SUBJECT TERMS Modeling Code, Thermochemical Erosion, Erosion Predictions, Gun Barrels, Thermochemical Ablation, Mechanical Erosion, M242/M919 Gun System, Chromium, Tantalum		15. NUMBER OF PAGES 26	
		16. PRICE CODE	
17. SECURITY CLASSIFICATION OF REPORT UNCLASSIFIED	18. SECURITY CLASSIFICATION OF THIS PAGE UNCLASSIFIED	19. SECURITY CLASSIFICATION OF ABSTRACT UNCLASSIFIED	20. LIMITATION OF ABSTRACT UL

TABLE OF CONTENTS

	<u>Page</u>
INTRODUCTION	1
THEORY AND PROCEDURE	1
RESULTS AND DISCUSSION	3
REFERENCES	8

LIST OF ILLUSTRATIONS

1. M919 XKTC Gas Pressures	10
2. M919 XKTC Gas Temperatures	11
3. M919 XKTC Gas Velocities	12
4. M919 MABL Recovery Enthalpies	13
5. M919 MABL Cold Wall Heats	14
6. M919 CCET Reacting Wall Enthalpies	15
7. M919 CCET Ablation and Melting Potential	16
8. M919 MACE Exposed Area of Subsurface A723	17
9. M919 MACE Second Variation of Exposed Area of Subsurface A723	18
10. M919 MACE Axial/Circumferential Depth Profile of Subsurface A723	19
11. M919 MACE 6" RFT Maximum Wall Temperatures	20
12. M919 MACE 12" RFT Maximum Wall Temperatures	21
13. M919 MACE 30" RFT Maximum Wall Temperatures	22
14. M919 MACE 6" Cumulative Erosion-to-Condemnation	23
15. M919 MACE 12" Cumulative Erosion-to-Condemnation	24
16. M919 MACE 30" Cumulative Erosion-to-Condemnation	25

INTRODUCTION

The study of chemical reactions in flow systems (aerothermochemistry) was first described by von Karman in 1951 (ref 1). The modification of the heat transfer coefficient (blocking) for the mass addition of chemically reacting wall material into the boundary layer was first described by Reshotko and Cohen in 1955 (refs 2,3). The thermochemical erosion of reentry vehicle heat shield material for various chemically reacting systems was first studied by Denison and Dooley in 1957 (ref 4). This thermochemical erosion theory was unified/summarized by Lees of CalTech and The Ramo-Wooldridge Corporation in 1958 (ref 5). The near exclusive use of Lees' now JANNAF standardized model (refs 6-8) has stood the test of time and demonstrates that the major assumptions are still reasonable and valid.

Gun barrel technology has focused on reducing mechanical/metallurgical gun barrel failures with great success, while gun barrel gas-wall thermochemical/thermal ablation coupled with aerodynamic flow erosion has intensified due to performance requirements demanding the use of high-flame temperature propellants. Practical gun barrel design should address thermochemical and thermal ablation, although the latter constitutes a poor design since the proximity of the wall solidus temperature should be avoided.

In 1992, after an exhaustive search, the U.S. Army Benet Laboratories (Benet) teamed with Software and Engineering Associates (SEA) to successfully modify the JANNAF standard rocket erosion codes (TDK/MACE) (refs 6-9) into the first comprehensive gun barrel thermochemical erosion modeling code that addresses wall degradations due to thermal (transformations), thermochemical (reactions), and thermomechanical (cracking) effects coupled with pure mechanical erosion (high-speed flow, wear). SEA is the sole maintainer and developer of these rocket erosion codes. The compressible chemical equilibrium and transport (CCET) thermochemistry code is similar but much more robust than the nonideal gas thermochemical equilibrium (BLAKE) code (ref 10). The gun erosion analysis uses the standard interior ballistics gun code (XNOVAKTC) (ref 11) core flow data as input. In 1993, a joint SEA/Benet gun erosion workshop was held to introduce this code to the gun community (ref 9). Many ADPA Tri-Service sponsored gun erosion meetings have implied a thermochemical erosion mechanism for various gun systems including the M242/M919 gun system (refs 12,13). U.S. Army experimental data support the existence of gun barrel oxidation (ref 14). In July 1995, Benet and SEA jointly published (AIAA) the first known comprehensive gun barrel thermochemical erosion modeling code (ref 15).

THEORY AND PROCEDURE

This report models the original M242/M919 gun system. The original gun system consists of 100 percent HES9053 propellant, a Condition Code D, 3550°K flame temperature, and an unplated barrel life of about 400 to 500 rounds. This original system is not to be confused with the type classified M242/M919 gun system, which is the modified reduced-wear M919 with 45 percent HES9053/55 percent HC33 propellants, an ablative, and 3350°K flame temperature; M791's HC-33 propellant has a 3200°K flame temperature (ref 12).

This original M242/M919 gun system (ref 12) erosion analysis includes the following codes:

- Standard interior ballistics gun code (XNOVAKTC for core flow) (ref 11)
- Standard nonideal gas-wall thermochemical rocket code modified for guns (CCET for gas-wall transport/chemistry) (refs 6,8,9)
- Standard heat transfer modified by mass addition to boundary layer rocket code modified for guns (MABL for transport and cold/adiabatic wall properties) (refs 6,9)
- Standard wall material ablation conduction erosion rocket code modified for guns (MACE) (refs 7,9)

The XNOVAKTC code and its core flow output are well known to the gun community; see Reference 11 for further information.

The CCET code (refs 6,8,9) outputs gun system inert/reacting gas-wall enthalpy (H_{gw}), condensed phase products mass fraction (C_{cg}), and ablation potential (B_a) data as a function of pressure and temperature. Combustion product omissions and gas-wall reactivity are based on in-house experimental testing, proprietary communications, and a U.S. Army report (refs 9,14). The CCET code assumes that as the gas diffuses to the wall, it reacts to form products as follows:

$$B_a = (C_w - C_{cg})/C_g \quad (1)$$

where C_w is the mass fraction of wall material and C_g is the mass fraction of the gas edge (ref 9).

The MABL code (refs 6,9) outputs adiabatic wall recovery enthalpy (H_r) and adiabatic wall temperature (T_{aw}) data as a function of time and travel. The recovery enthalpy is the potential chemistry driver where the heat transfer approaches zero and the adiabatic wall temperature is the potential temperature without reactions. The MABL code also outputs cold wall heat transfer rate (Q_{cw}) data as a function of time and travel. This heat transfer rate is the wall heat flux evaluated at the cold wall temperature. The MABL code heat and mass transfer model includes the following three equations. The first equation is for mass addition to the boundary layer, the second equation is for heat-to-mass transfer ratio, and the third equation is for the overall correlation between the first and second equations:

$$r_e U_e Ch_o = Q_{cw}/(H_r - H_{gw}) \quad (2)$$

$$r_e U_e Ch_b = Mdot_g/B_a; Le = 1 \quad (3)$$

$$Ch_b/Ch_o = f(B_a, M_w) = 1 - (h Mdot_g/r_e U_e Ch_o) \quad (4)$$

where r_e is edge density, U_e is edge velocity, Ch_o is Stanton number without blowing, Q_{cw} is cold wall heat transfer, H_r is recovery enthalpy, H_{gw} is gas-wall enthalpy, Ch_b is Stanton number with blowing, $Mdot_g$ is gas mass transfer, Le is the Lewis number, B_a is ablation potential, M_w is molecular weight, and h is $f(G-BL)$ molecular diffusion) (ref 9).

The MACE code (refs 7,9) calculates the actual transient thermochemical response and generates wall material erosion predictions and comparisons (ablation, conduction, and erosion profiles) as a function of time, travel (customer-selected 6-inch, 12-inch, 30-inch), and number of rounds to barrel condemnation. The A723, 0.002-inch plated chromium/A723, and 0.002-inch sputtered tantalum/A723 wall materials are evaluated for maximum wall temperature and erosion using the M242 Cycle A firing scenario. The MACE code can do any propellant-gun barrel combination on a high end PC; each mechanism's importance is identified and incremental upgrades are feasible.

The original M242/M919 MACE maximum wall temperature gun system predictions are compared to those of the U.S. Army's standard gun barrel finite difference heat transfer code (FDHEAT) (ref 16) that calculates the transient temperature distribution in a multilayered cylinder and models radial/axial heat flow separately. The A723, 0.002-inch plated chromium/A723, and 0.002-inch sputtered tantalum/A723 wall materials are evaluated by FDHEAT for maximum wall temperature also using the M242 Cycle A firing scenario. The original M242/M919 gun system predictions are also compared to actual M919 A723 experimentally-measured gun system erosion data from an ARDEC Special Report for the Commander on the subject (ref 17).

RESULTS AND DISCUSSION

Figure 1 gives the calculated M919 XKTC gas pressures (P) as a function of time for the customer-selected axial positions. Figure 2 gives the calculated M919 XKTC gas temperatures (T) as a function of time for these same positions. Figure 3 gives the calculated M919 XKTC gas velocities (V) as a function of time again for these same positions.

Figure 4 gives the calculated M919 MABL recovery enthalpies (H_r) as a function of time for the same customer-selected axial positions above. Figure 5 gives the calculated M919 MABL cold wall heats (Q_{cw}) as a function of time for these same positions. The data in Figures 4 and 5 are two of three parts of the driving potential (Q/dH), which is essentially mass affected per the quantity area times time.

Figure 6 gives the calculated M919 CCET reacting wall enthalpies (H_{gw}) for tantalum, chromium, and A723 as a function of temperature. The figure includes the third of three parts of the driving potential (Q/dH), which again is essentially mass affected per the quantity area times time. Figure 7 gives the calculated M919 CCET ablation and melting potential (B_a) for tantalum, chromium, and A723 as a function of temperature. Figures 6 and 7 show that tantalum metal oxidizes at $3100^\circ R$ ($2610^\circ F$), its oxide melts at $3860^\circ R$ ($3370^\circ F$), and it melts at $5880^\circ R$ ($5390^\circ F$). Figures 6 and 7 show that chromium metal oxidizes at $3600^\circ R$ ($3110^\circ F$), it has a

solid-solid transformation at 3790° R (3300° F), it melts at 3830° R (3340° F), and its oxide melts at 4570° R (4080° F). Figures 6 and 7 show that A723 steel has a solid-solid transformation at 1800° R (1310° F), it oxidizes at 1900° R (1410° F), its oxide melts at 2960° R (2460° F), and it melts at 3250° R (2760° F). These two figures show that both tantalum and A723 walls oxidize substantially below their melting points, while the chromium wall oxidizes just below its melting point, but they also show that only the A723 wall oxidation is important since the intensity of the oxidation renders the tantalum and chromium walls essentially inert to oxidation. Similarly, these two figures show that both tantalum and A723 wall oxides melt well below their metals, while the chromium wall oxide melts well above chromium metal, but they also show that only the A723 wall oxide melting is important since the intensity of the oxidation/oxide melting renders the tantalum and chromium walls essentially inert to oxidation/oxide melting.

Figure 8 shows the calculated M919 MACE exposed area of subsurface A723 steel, where recurring bore protection material plate areas of 0.0035-in.² and 0.0075-in.² are compared for a constant recurring 0.0080-in.² total area and a 0.0005-inch crack width. For the 0.0035-in.² plates, which are typical for M919 chromium/A723 bore protection by metallography and modeling (refs 18,19), cracks consume 23 percent of the total area and plates consume 77 percent of the total area. Also, for the 0.0035-in.² plates, half the subsurface A723 under a given plate (0.0025-in.²) is consumed in 1x rounds, and at this point metallography and modeling tell us the plate spalls (refs 18,19). For the 0.0075-in.² plates, which are typical for M919 tantalum/A723 bore protection by metallography and modeling (refs 18,19), cracks consume 12 percent of the total area and plates consume 88 percent of the total area. Also, for the 0.0075-in.² plates, half the subsurface A723 under a given plate (0.0055-in.²) is consumed in 2x rounds, and at this point metallography and modeling tell us the plate spalls (refs 18,19). Although both have 0.0005-inch crack width with 0.0035-in.² plates typical for chromium/A723 and 0.0075-in.² plates typical for tantalum/A723, each represents a sensitivity analysis for the other with respect to plate width for a recurring total area.

Figure 9 shows the calculated M919 MACE second variation of exposed area of subsurface A723 steel, where recurring bore protection material plate areas of 0.00375-in.² and 0.00775-in.² are compared for a constant recurring 0.0080-in.² total area and a 0.00025-inch crack width. For the 0.00375-in.² plates, which are atypical for M919 bore protection by metallography and modeling (refs 18,19), cracks consume 12 percent of the total area and plates consume 88 percent of the total area. Also, for the 0.00375-in.² plates, half the subsurface A723 under a given plate (0.0027-in.²) is consumed in 2x rounds, and at this point metallography and modeling tell us the plate spalls (refs 18,19). For the 0.00775-in.² plates, which are atypical for M919 bore protection by metallography and modeling (refs 18,19), cracks consume 6 percent of the total area and plates consume 94 percent of the total area. Also, for the 0.00775-in.² plates, half the subsurface A723 under a given plate (0.0056-in.²) is consumed in 4x rounds, and at this point metallography and modeling tell us the plate spalls (refs 18,19). Although both have 0.00025-inch crack width with 0.00375-in.² plates atypical and 0.00775-in.² plates atypical, each represents

a sensitivity analysis for the other with respect to plate width for a recurring total area. In addition, 0.0005-inch crack width from Figure 8 and 0.00025-inch crack width from Figure 9, with variation in plate area within the same recurring total area, represent a sensitivity analysis with respect to crack width for the recurring total area.

Figure 10 shows the calculated M919 MACE axial/circumferential depth profile of subsurface A723 steel, where typical recurring bore protection material plate areas of 0.0035-in.² for chromium/A723 and 0.0075-in.² for tantalum/A723 are compared for a constant recurring 0.0080-in.² total area and a typical 0.0005-inch crack width. Viewing the upper part of this figure in the two dimensions shown for the typical M919 0.002-inch chromium plate depth and 0.0035-in.² chromium plates, shows it takes 1x rounds for a pair of 0.001-inch deep by 0.0018-inch wide average A723 voids to occur below both crack chromium/A723 interfaces of this 0.0035-in.² chromium plate. This causes the plate to spall since half the area under the plate is consumed as discussed earlier. Viewing the lower part of this figure in the two dimensions shown for the typical M919 0.002-inch tantalum plate depth and 0.0075-in.² tantalum plates, shows it takes 2x rounds for a pair of 0.001-inch deep by 0.0035-inch wide average A723 voids to occur below both crack tantalum/A723 interfaces of this 0.0075-in.² tantalum plate. This plate also spalls since half the area under the plate is consumed as discussed earlier. Variation of exposed area of subsurface A723 varies its Q_{in} , T_{in} , and driving potential (Q/dH).

Figure 11 gives the calculated M919 MACE 6-inch axial position from RFT maximum wall temperatures as a function of rounds for the M919 Cycle A 150-round firing scenario. The MACE code-generated tantalum/A723 wall curve achieved the highest temperatures, and the FDHEAT code (ref 16)-generated tantalum/A723 wall curve shows good agreement. The MACE code-generated chromium/A723 wall curve achieved the second highest temperatures, and the FDHEAT code (ref 16)- generated tantalum/A723 wall curve again shows good agreement. The MACE code-generated A723 wall curve achieved the third highest temperatures; the MACE code-generated chromium/A723 interface wall curve achieved the fourth highest temperatures; and the MACE code-generated tantalum/A723 interface wall curve achieved the lowest temperatures. The highly verified FDHEAT code is considered the U.S. Army standard code for wall temperature predictions (ref 16). No FDHEAT code data were available to compare these last three wall types. This figure distinctly shows that all the A723, chromium/A723 interface, and tantalum/A723 interface wall curves significantly exceed both the 1310° F A723 solid-solid transformation and the 1410° F A723 oxidation temperatures. The figure further shows that all other metal solid-solid transformation temperatures, all other metal oxidation temperatures, all metal oxide melting, and all metal melting are significantly above the temperatures given for the plotted curves in the 2460° to 5390° F range. Clearly, at 6 inches, tantalum and chromium are thermochemically inert for this analysis, but their A723 interfaces and A723 itself are substantially thermochemically reactive.

Figure 12 gives the calculated M919 MACE 12-inch axial position from RFT maximum wall temperatures as a function of rounds for the M919 Cycle A 150-round firing scenario. The MACE code-generated tantalum/A723 wall curve again achieved the highest temperatures, and

the FDHEAT code (ref 16)-generated tantalum/A723 wall curve shows good agreement. The MACE code-generated chromium/A723 wall curve again achieved the second highest temperatures, with the FDHEAT code (ref 16)-generated chromium/A723 wall curve showing good agreement. The MACE-code generated A723 wall curve again achieved the third highest temperatures; the MACE-code generated chromium/A723 interface wall curve achieved the fourth highest temperatures; and the MACE-code generated tantalum/A723 interface wall curve achieved the lowest temperatures. Additionally, no FDHEAT code data were available to compare these last three wall types. This figure clearly shows that all the A723, chromium/A723 interface, and tantalum/A723 interface wall curves exceed both the 1310° F A723 solid-solid transformation and the 1410° F A723 oxidation temperatures. The figure further shows that all other metal solid-solid transformation temperatures, all other metal oxidation temperatures, all metal oxide melting, and all metal melting are significantly above the temperatures given for the plotted curves in the 2460° to 5390° F range. Clearly, at 12 inches, tantalum and chromium are thermochemically inert for this analysis, but their A723 interfaces and A723 itself are substantially thermochemically reactive.

Figure 13 gives the calculated M919 MACE 30-inch axial position from RFT maximum wall temperatures as a function of rounds for the M919 Cycle A 150-round firing scenario. The MACE code-generated tantalum/A723 wall curve again achieved the highest temperatures; the MACE code-generated chromium/A723 wall curve achieved the second highest temperatures; the MACE code-generated A723 wall curve achieved the third highest temperatures; the MACE code-generated chromium/A723 interface wall curve achieved the fourth highest temperatures; and the MACE code-generated tantalum/A723 interface wall curve achieved the lowest temperatures. No FDHEAT code data were available to compare these five wall types. This figure clearly shows that the all of the A723 wall curve, half of the chromium/A723 interface wall curve, and half of the tantalum/A723 interface wall curve exceed the 1310° F A723 solid-solid transformation temperature. Also, this figure shows that most of the A723 wall curve, none of the chromium/A723 interface wall curve, and none of the tantalum/A723 interface wall curve exceed the 1410° F A723 oxidation temperature. The figure further shows that all other metal solid-solid transformation temperatures, all other metal oxidation temperatures, all metal oxide melting, and all metal melting are significantly above the temperatures given for the plotted curves in the 2460° to 5390° F range. Clearly, at 30 inches, tantalum, chromium, and their A723 interfaces are thermochemically inert for this analysis. Although A723 itself is thermochemically reactive, there is no mechanism to consume/spall the tantalum or chromium for this reactivity to occur.

Figure 14 gives the calculated M919 MACE 6-inch cumulative erosion-to-condemnation as a function of rounds. The eight curves will be discussed in order of increasing rounds-to-condemnation. The first curve, labeled "A723, Ref" is actually M919 A723 experimentally-measured gun system erosion data from an ARDEC Special Report for the Commander (ref 17). The system, removed from service at 205 rounds, reaches condemnation at 370 rounds by extrapolation, and agrees rather well with the MACE-generated A723 curve shown. The second curve is the MACE-generated A723 curve that shows condemnation at 444 rounds. The third

curve is the MACE-generated typical chromium/A723 interface curve for a 0.0035-in.² chromium plate/0.0005-inch crack width that shows interface failure/chromium spalling at 370 rounds and condemnation at 814 rounds. The fourth curve is the MACE-generated atypical chromium/A723 interface curve for a 0.0070-in.² chromium plate/0.0005-inch crack width, showing interface failure/chromium spalling at 740 rounds and condemnation at 1184 rounds. This curve is provided for sensitivity analysis purposes. The fifth curve is the MACE-generated typical tantalum/A723 interface curve for a 0.0070-in.² tantalum plate/0.0005-inch crack width, showing interface failure/tantalum spalling at 909 rounds and condemnation at 1353 rounds. The sixth curve is the MACE-generated atypical tantalum/A723 interface curve for a 0.0140-in.² tantalum plate/0.0005-inch crack width that shows interface failure/tantalum spalling at 1818 rounds and condemnation at 2262 rounds. This curve is also provided for sensitivity analysis purposes. The seventh and eighth curves are the MACE-generated typical chromium/A723 and tantalum/A723 curves that superimpose and have virtually no cumulative erosion for the purposes of this analysis.

Figure 15 gives the calculated M919 MACE 12-inch cumulative erosion-to-condemnation as a function of rounds. The five curves will be discussed in order of increasing rounds-to-condemnation. The first curve is the MACE-generated A723 curve that shows condemnation at 1000 rounds. The second curve is the MACE-generated typical chromium/A723 interface curve for a 0.0035-in.² chromium plate/0.0005-inch crack width that shows interface failure/chromium spalling at 1515 rounds and condemnation at 2515 rounds. The third curve is the MACE-generated typical tantalum/A723 interface curve for a 0.0070-in.² tantalum plate/0.0005-inch crack width, showing interface failure/tantalum spalling at 5882 rounds and condemnation at 6882 rounds. The fourth and fifth curves are the MACE-generated typical chromium/A723 and tantalum/A723 curves that superimpose and have virtually no cumulative erosion for the purposes of this analysis.

Figure 16 gives the calculated M919 MACE 30-inch cumulative erosion-to-condemnation as a function of rounds. The five curves will be discussed in order of increasing rounds-to-condemnation. The first curve is the MACE-generated A723 curve that shows condemnation at 5263 rounds. The second through fifth curves are the MACE-generated typical chromium/A723 interface curve for a 0.0035-in.² chromium plate/0.0005-inch crack width, typical tantalum/A723 interface curve for a 0.0070-in.² tantalum plate/0.0005-inch crack width, typical chromium/A723, and typical tantalum/A723 curves that superimpose and have virtually no cumulative erosion for the purposes of this analysis.

REFERENCES

1. von Karman, T., *Sorbonne Lectures*, 1951-1952; see also *Princeton University Lectures*, 1953; "Fundamental Approach to Laminar Flame Propagation," *AGARD Selected Combustion Problems*, Butterworths, London, 1954; and "Fundamental Equations in Aerothermochemistry," *Proc. 2nd AGARD Combust. Colloq.*, Liege, Belgium, 1955.
2. Reshotko, E., and Cohen, C.B., "Heat Transfer at the Stagnation Point of Blunt Bodies," NACA TN Number 3513, July 1955.
3. Cohen, C.B., Bromberg, R., and Lipkis, R.P., "Boundary Layers with Chemical Reactions Due to Mass Additions," Report No. GM-TR-268, The Ramo-Wooldridge Corporation, Los Angeles, CA, 1957.
4. Denison, M.R., and Dooley, D.A., "Combustion in the Laminar Boundary Layer of Chemically Active Sublimators," Publication No. C-110, Aeronutronic Systems, Inc., Glendale, CA, 1957.
5. Lees, L., "Convective Heat Transfer with Mass Addition and Chemical Reactions," *Combustion and Propulsion, Proc. 3rd AGARD Combust. Colloq.*, Palermo, Sicily, Pergamon Press, NY, 1958; see also *Recent Advances in Heat and Mass Transfer*, McGraw-Hill, NY, 1961.
6. Nickerson, G., Berker, D., Coats, D., and Dunn, S., "Two-Dimensional Kinetics (TDK) Nozzle Performance Computer Program," Software and Engineering Associates, Inc., Carson City, NV, 1993.
7. Dunn, S., "Materials Ablation Conduction Erosion Program (MACE)," Software and Engineering Associates, Inc., Carson City, NV, 1989.
8. Gordon, S., and McBride, B., "Computer Program for Calculation of Complex Chemical Equilibrium Compositions, Rocket Performance, Incident and Reflected Shocks, and Chapman-Jouguet Detonations (CET)," NASA SP-273, NASA Lewis Research Center, Cleveland, OH, 1971.
9. Dunn, S., and Sopok, S., Private Communications: Modification of the TDK/MACE Rocket Erosion Code to the Gun Barrel Erosion Code and Workshops on Gun Barrel Erosion, Software and Engineering Associates, Inc., Carson City, NV, and U.S. Army Benet Laboratories, Watervliet, NY, 1992-1993.
10. Freedman, E., "BLAKE - A Thermodynamic Code Based on Tiger: User's Guide and Manual," Technical Report ARBRL-TR-02411, U.S. Army Ballistic Research Laboratory, Aberdeen Proving Ground, MD, 1982.

11. Gough, P., "The XNOVAKTC Code," Paul Gough Associates, Portsmouth, NH, 1990.
12. 25-mm M242 Bushmaster Gun System Drawings, U.S. Army ARDEC, Dover, NJ, 1991-1996.
13. Picard, J., Ahmad, I., and Bracuti, A., *Proceedings of the Tri-Service Gun Tube Wear and Erosion Symposiums*, U.S. Army ARDEC/ADPA, Dover, NJ, 1970, 1972, 1977, and 1982.
14. Alkidas, A., Morris, S., Christoe, C., Caveny, L., and Summerfield, M., "Erosive Effects of Various Pure and Combustion-Generated Gases on Metals - Part II," U.S. Army Materials and Mechanics Research Center, Watertown, MA, 1977; see also Part I, 1975.
15. Dunn, S., Sopok, S., Coats, D., O'Hara, P., Nickerson, G., and Pflegl, G., "Unified Computer Model for Predicting Thermochemical Erosion In Gun Barrels," *Proceedings of 31st AIAA Joint Propulsion Conference*, San Diego, CA, July 1995.
16. Witherell, M., Private Communications: FDHEAT Code, U.S. Army Benet Laboratories, Watervliet, NY, 1995-1996.
17. Capsimalis, G., Cox, J., O'Hara, P., Witherell, M., Sopok, S., Underwood, J., Pflegl, G., and Cote, P., "Benet Laboratories M242/M919 Multi-Disciplinary Analyses," U.S. Army ARDEC Special Report for Commander, Benet Laboratories, Watervliet, NY, 1992.
18. Rickard, C., Private Communications: M242 Metallographic Analyses, U.S. Army Benet Laboratories, Watervliet, NY, 1995-1996.
19. Parker, T., and Underwood, J., Private Communications: Bore Protection Material Crack Modeling, U.S. Army Benet Laboratories, Watervliet, NY, 1995-1996.

Figure 1 - M919 XKTC Gas Pressures

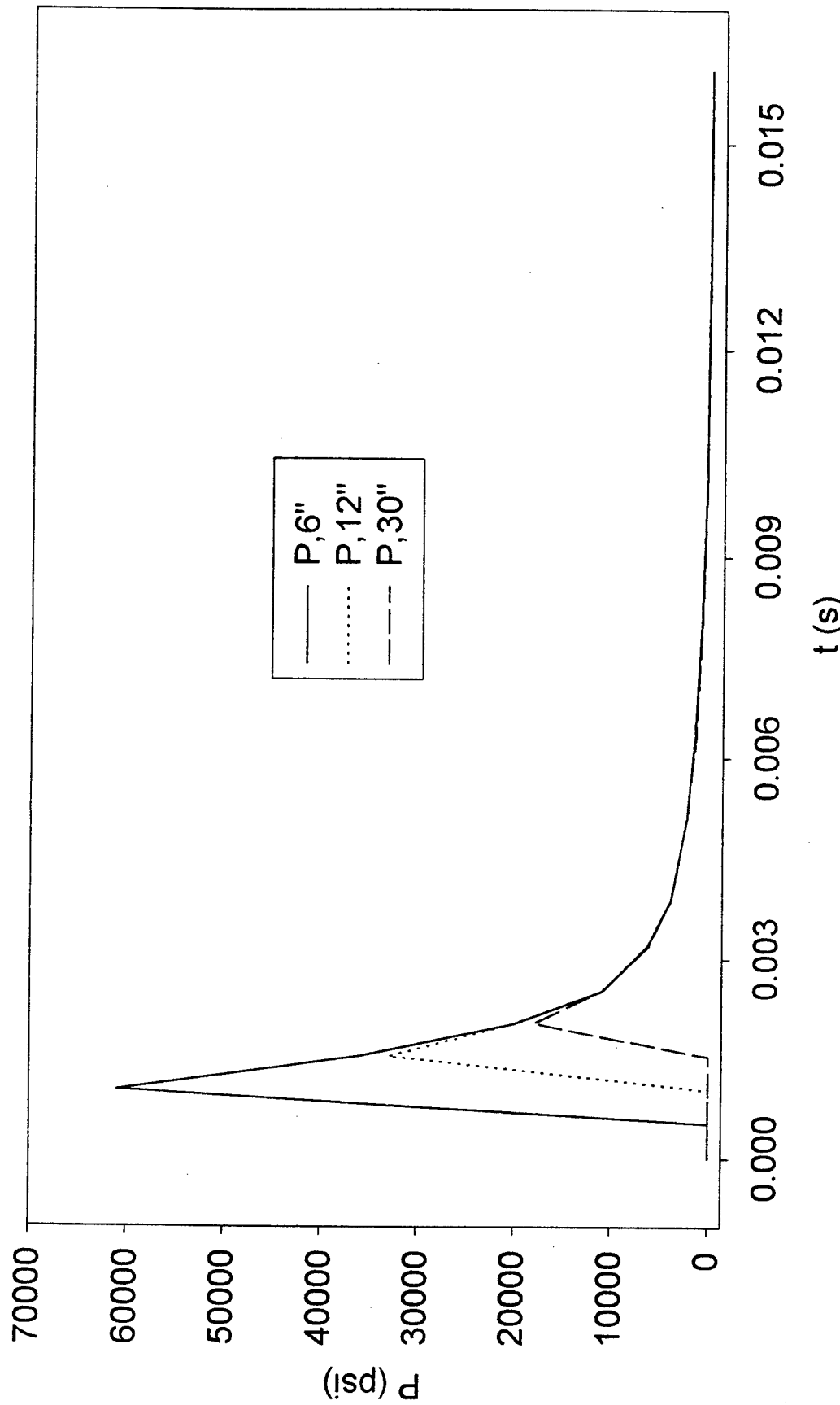


Figure 2 - M919 XKTC Gas Temperatures

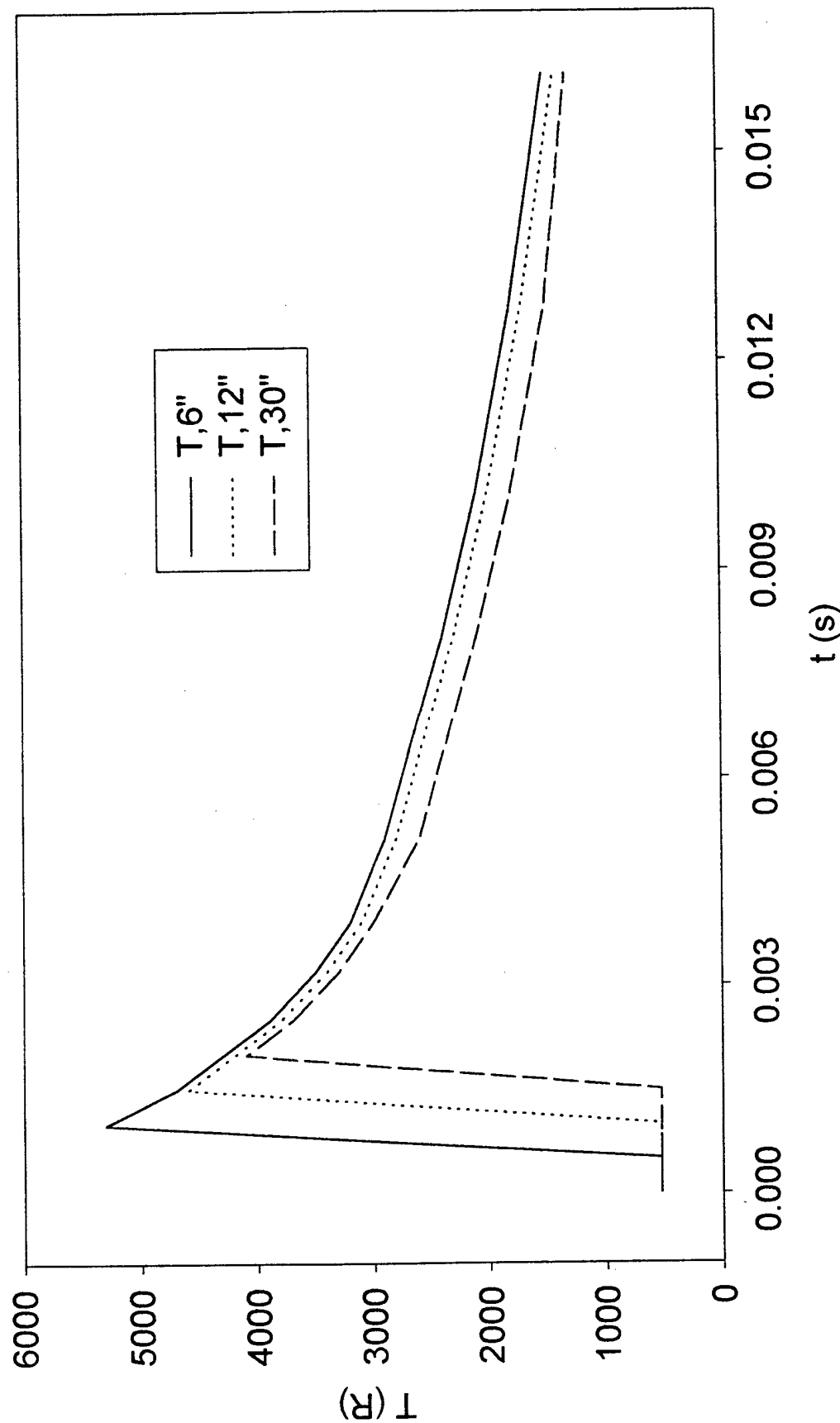


Figure 3 - M919 XKTC Gas Velocities

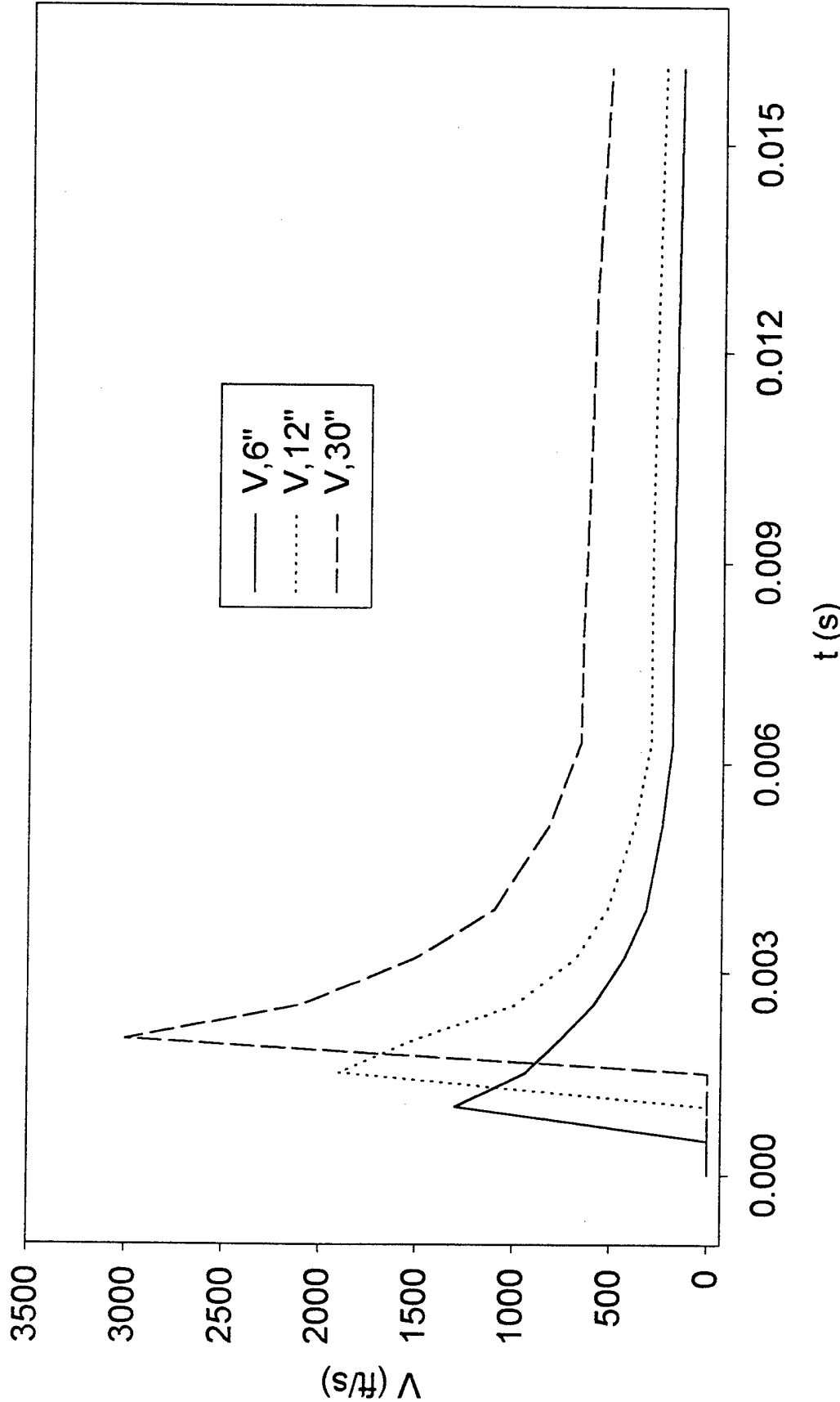


Figure 4 - M919 MABL Recovery Enthalpies
(Q / dH = Mass Affected / Area Time = Driving Potential)

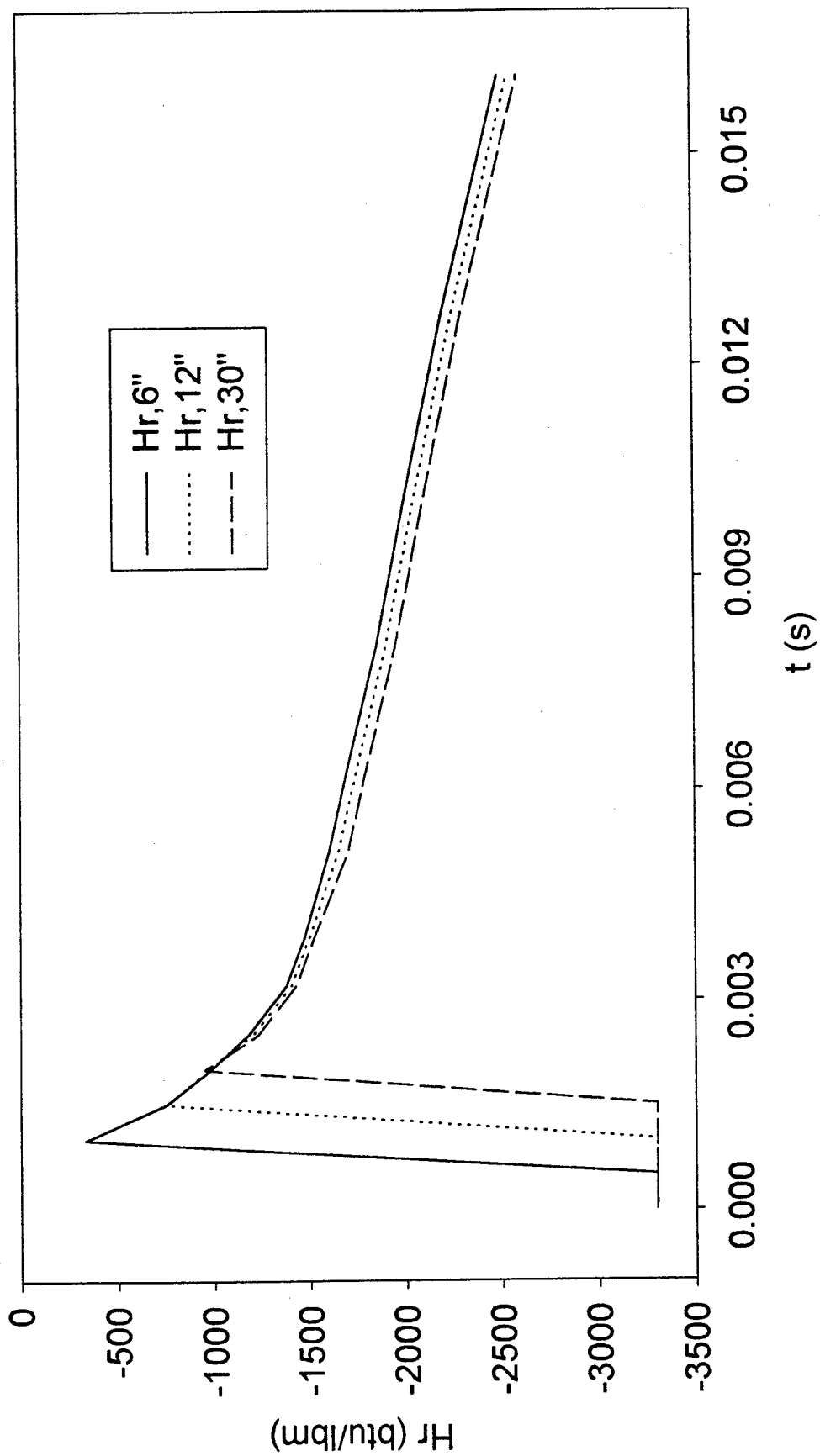


Figure 5 - M919 MABL Cold Wall Heats
(Q / dH = Mass Affected / Area Time = Driving Potential)

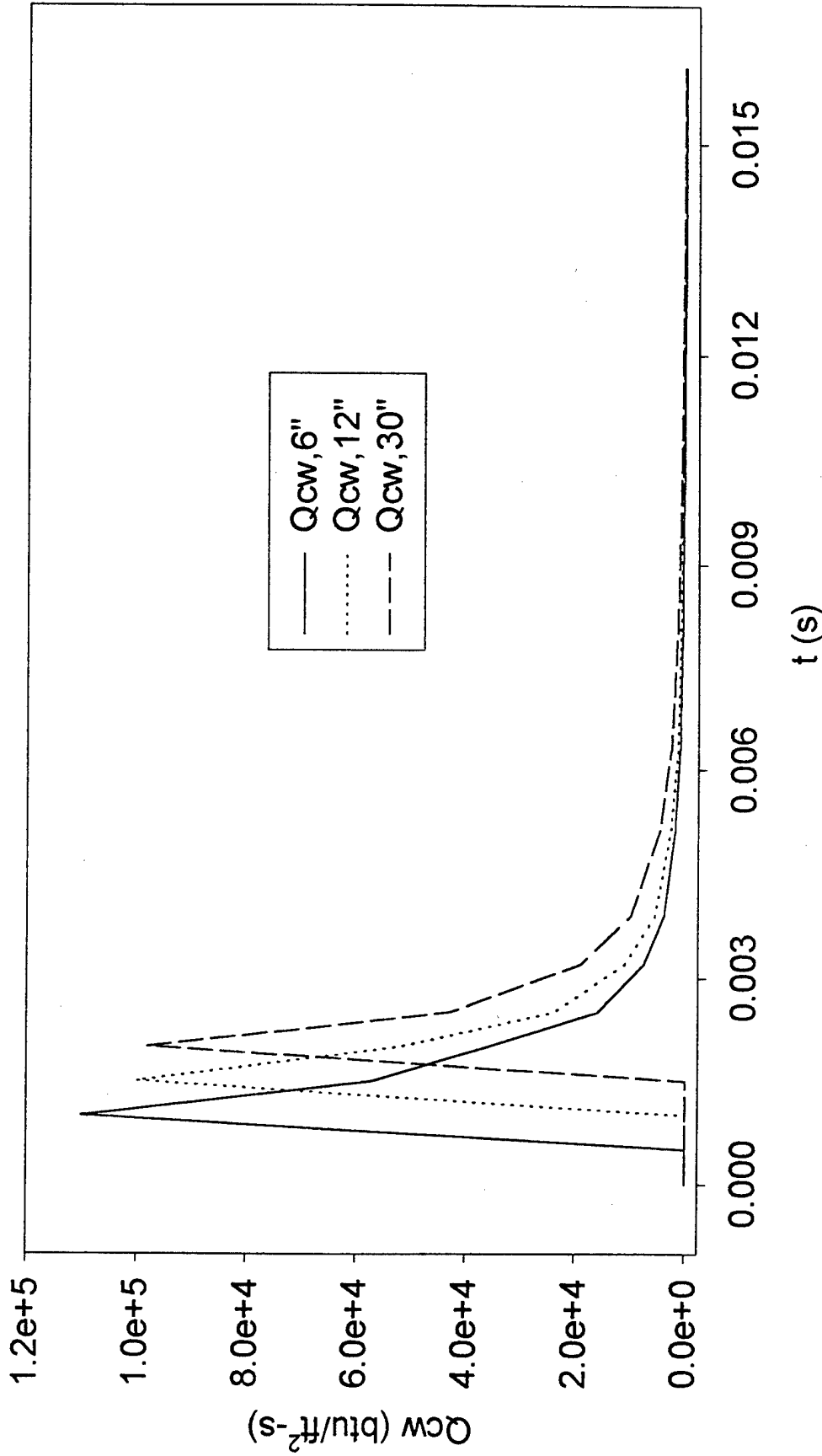


Figure 6 - M919 CCET Reacting Wall Enthalpies

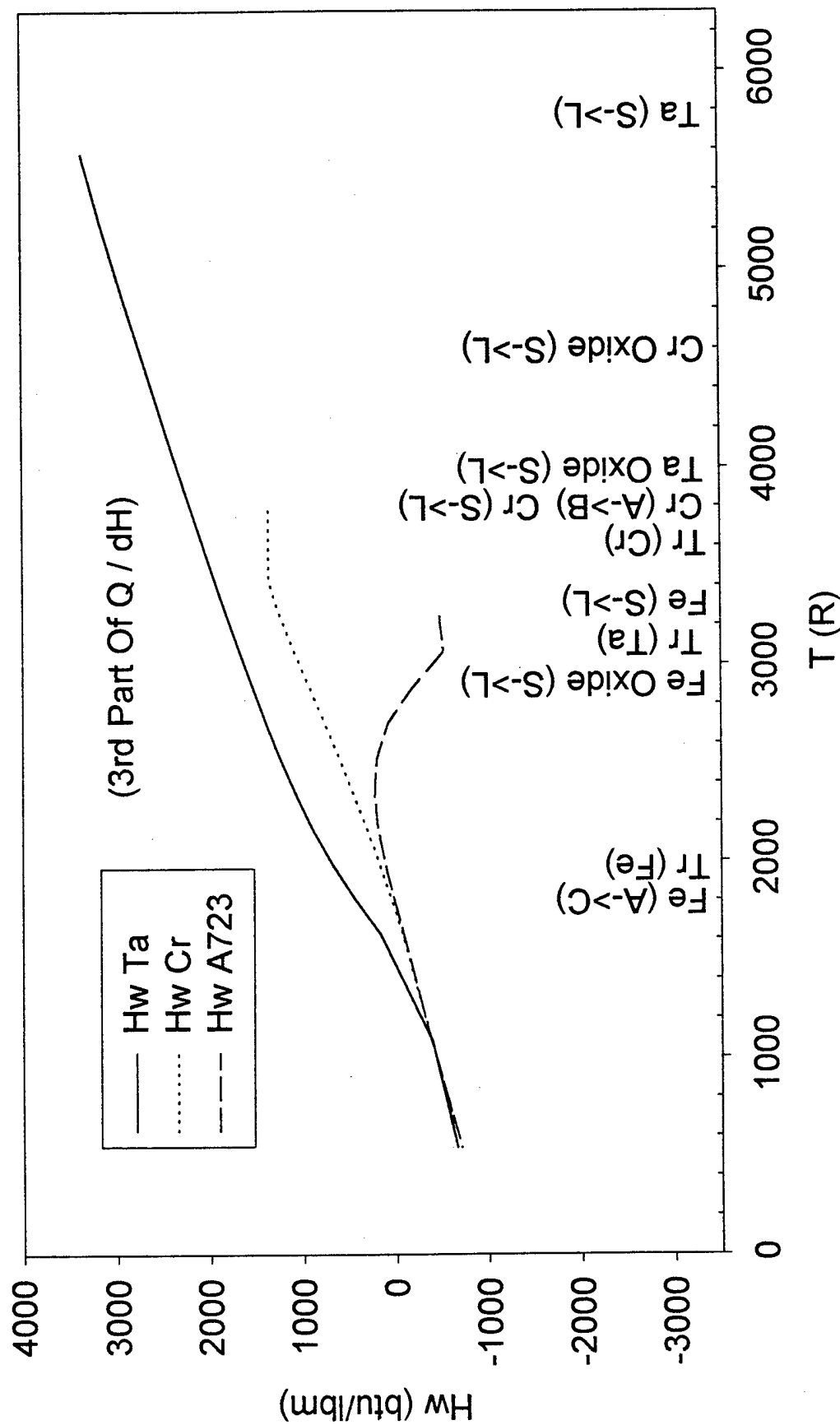


Figure 7 - M919 CCET Ablation & Melting Potential

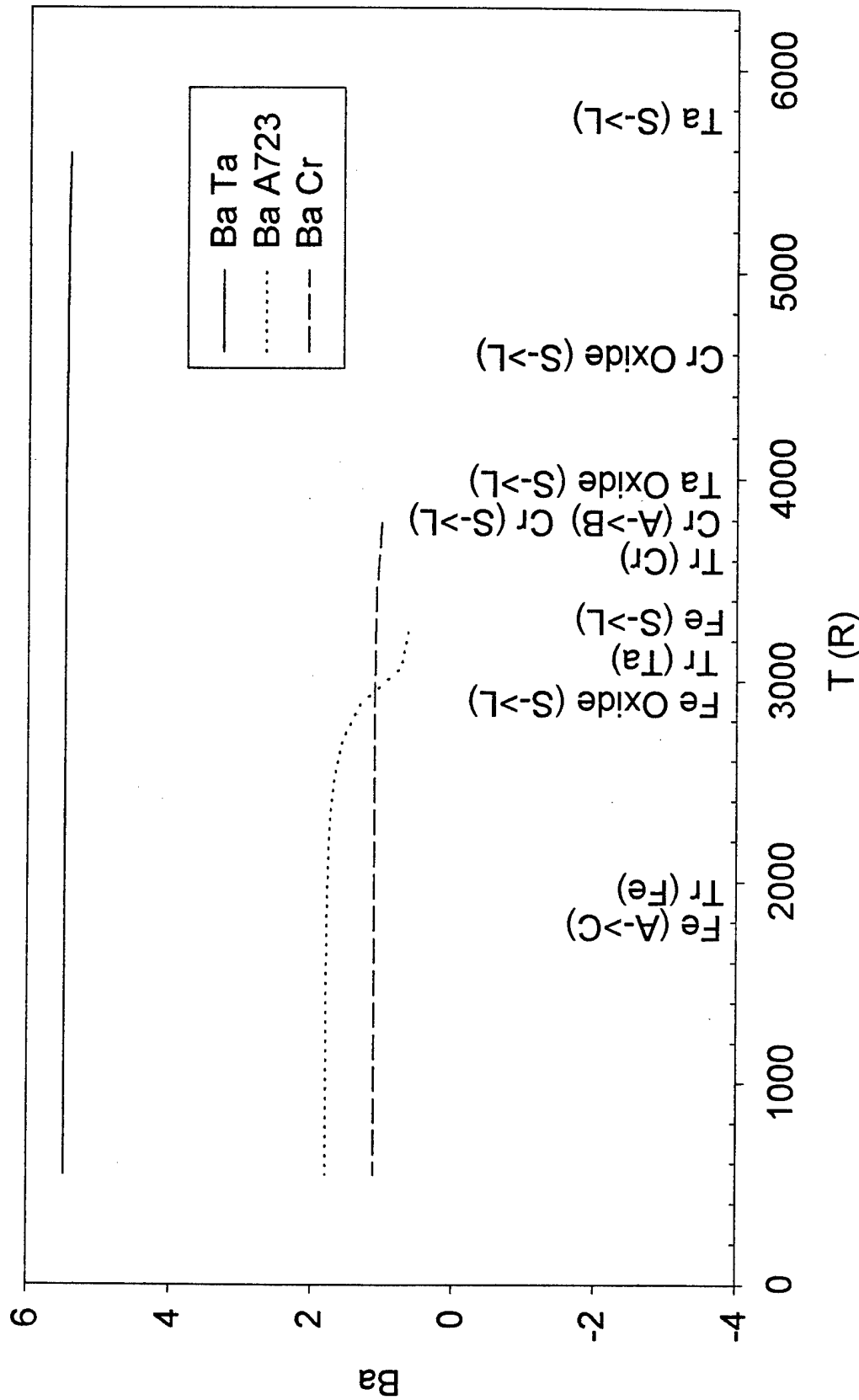


Figure 8 - M919 MACE Exposed Area Of Subsurface A723

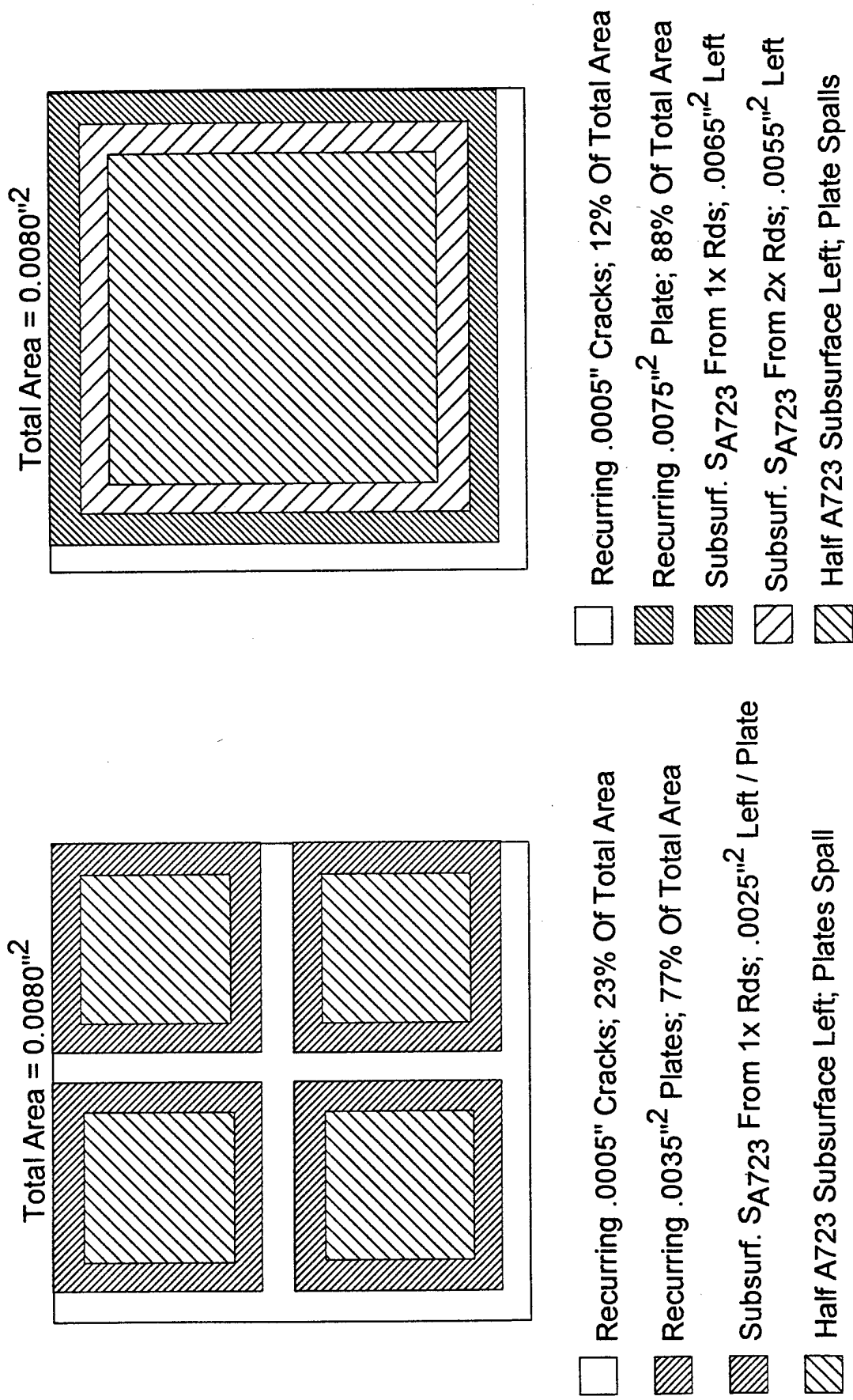
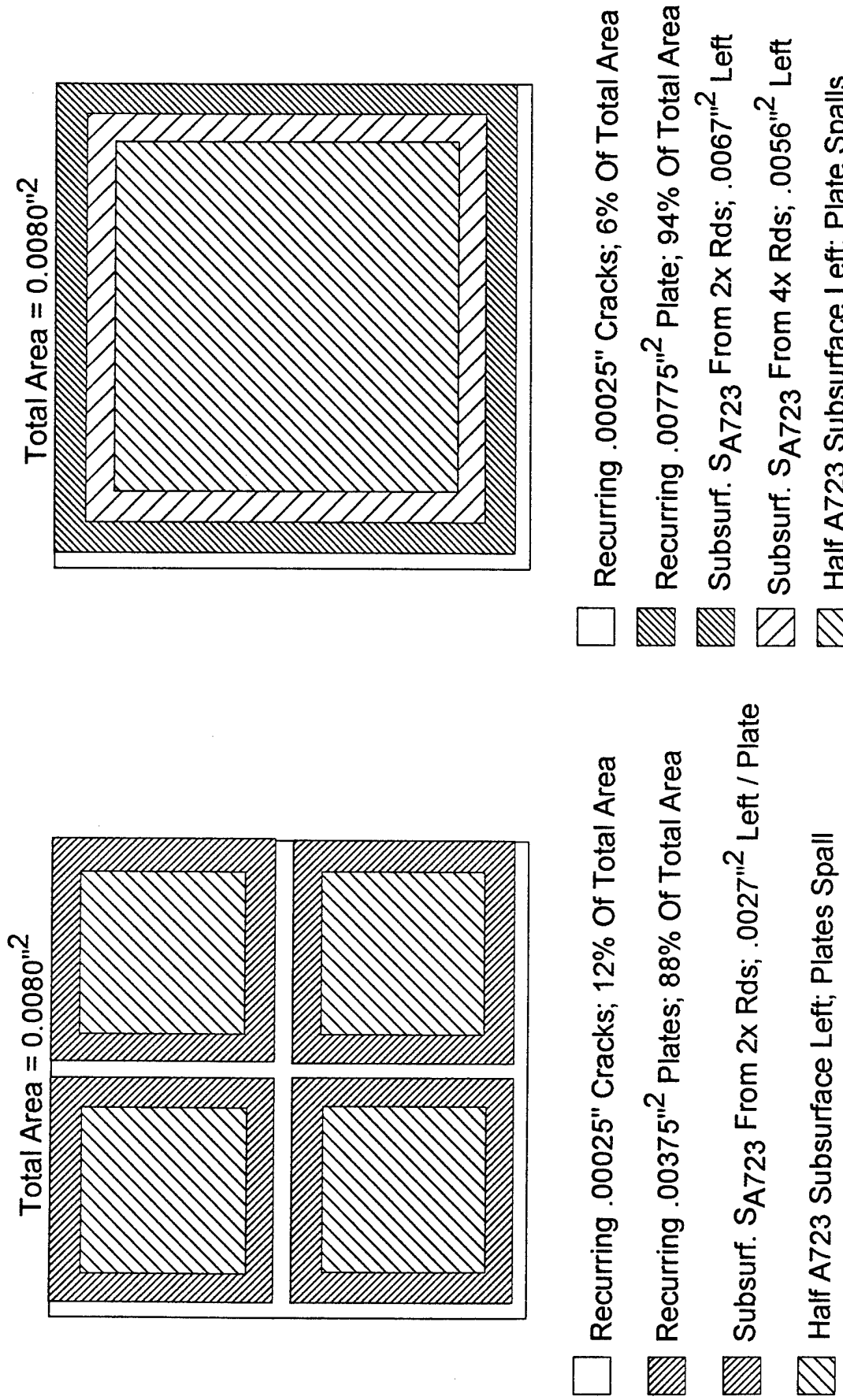
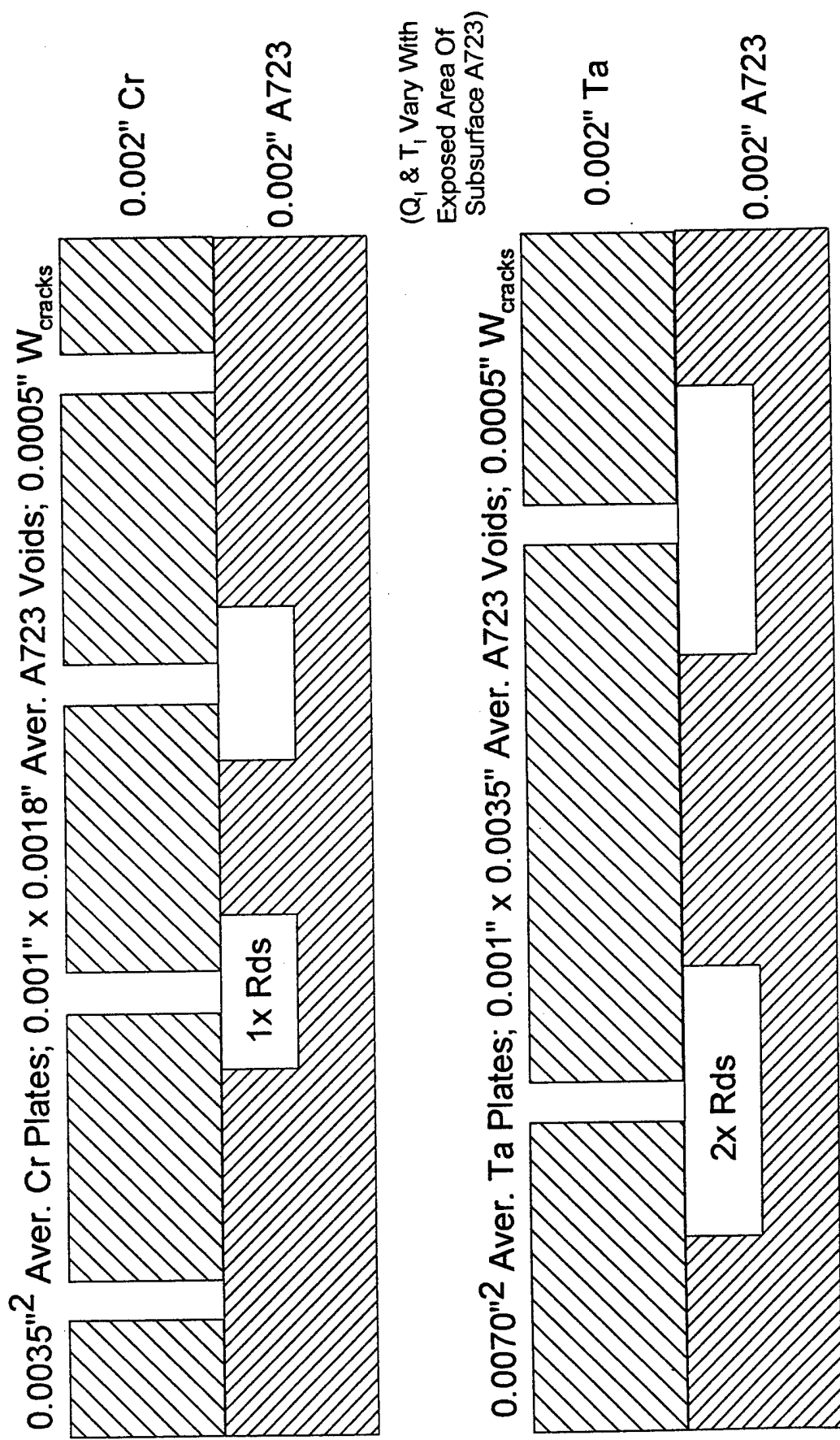


Figure 9 - M919 MACE Second Variation Of Exposed Area Of Subsurface A723



Acknowledgements: Rickard for Metallography; Also Parker & Underwood for Crack Modeling

Figure 10 - M919 MACE Axial/Circum. Depth Profile Of Subsurface A723



Acknowledgements: Rickard for Metallography; Also Parker & Underwood for Crack Modeling

Figure 11 - M919 MACE 6" RFT Maximum Wall Temperatures

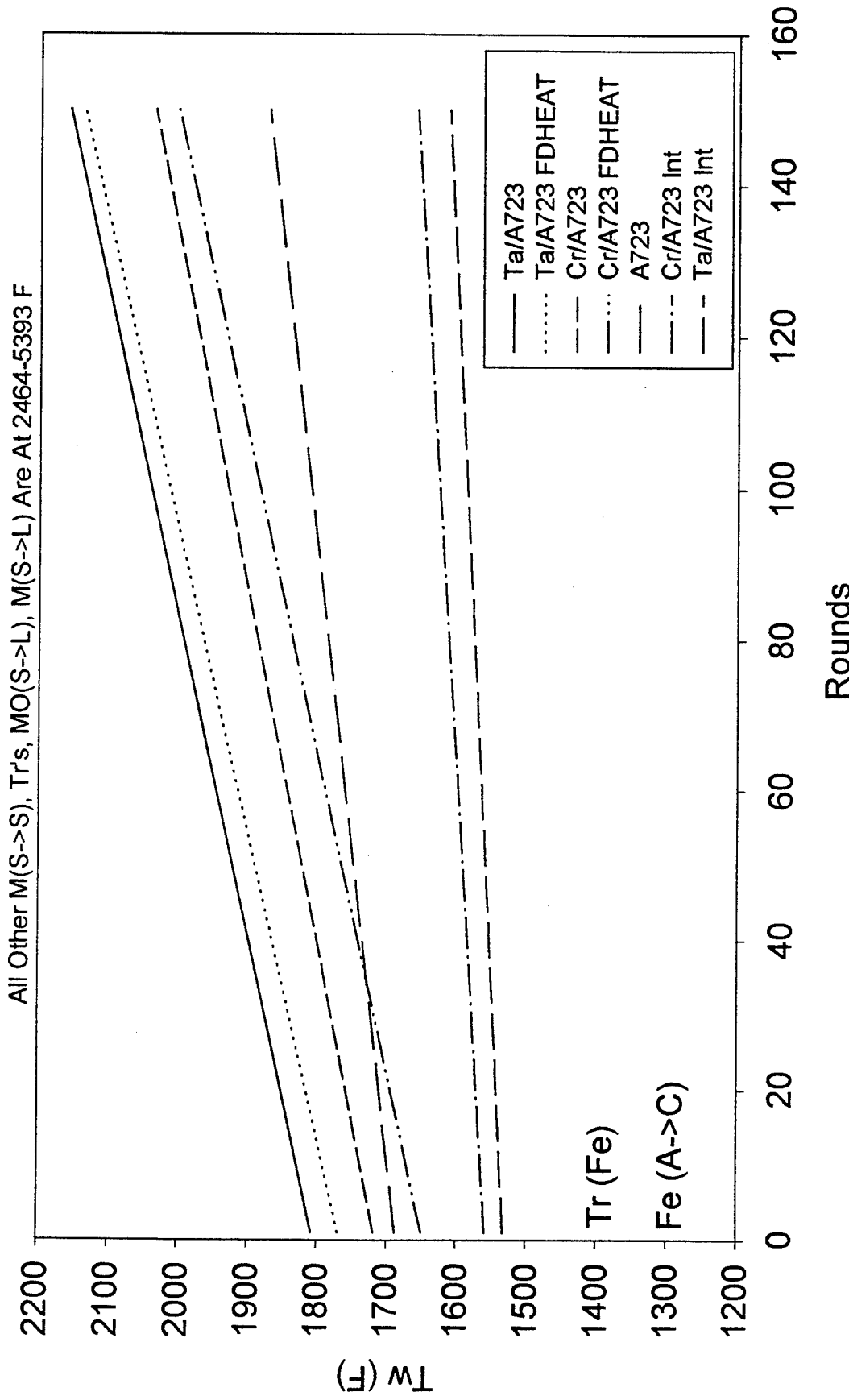


Figure 12 - M919 MACE 12" RFT Maximum Wall Temperatures

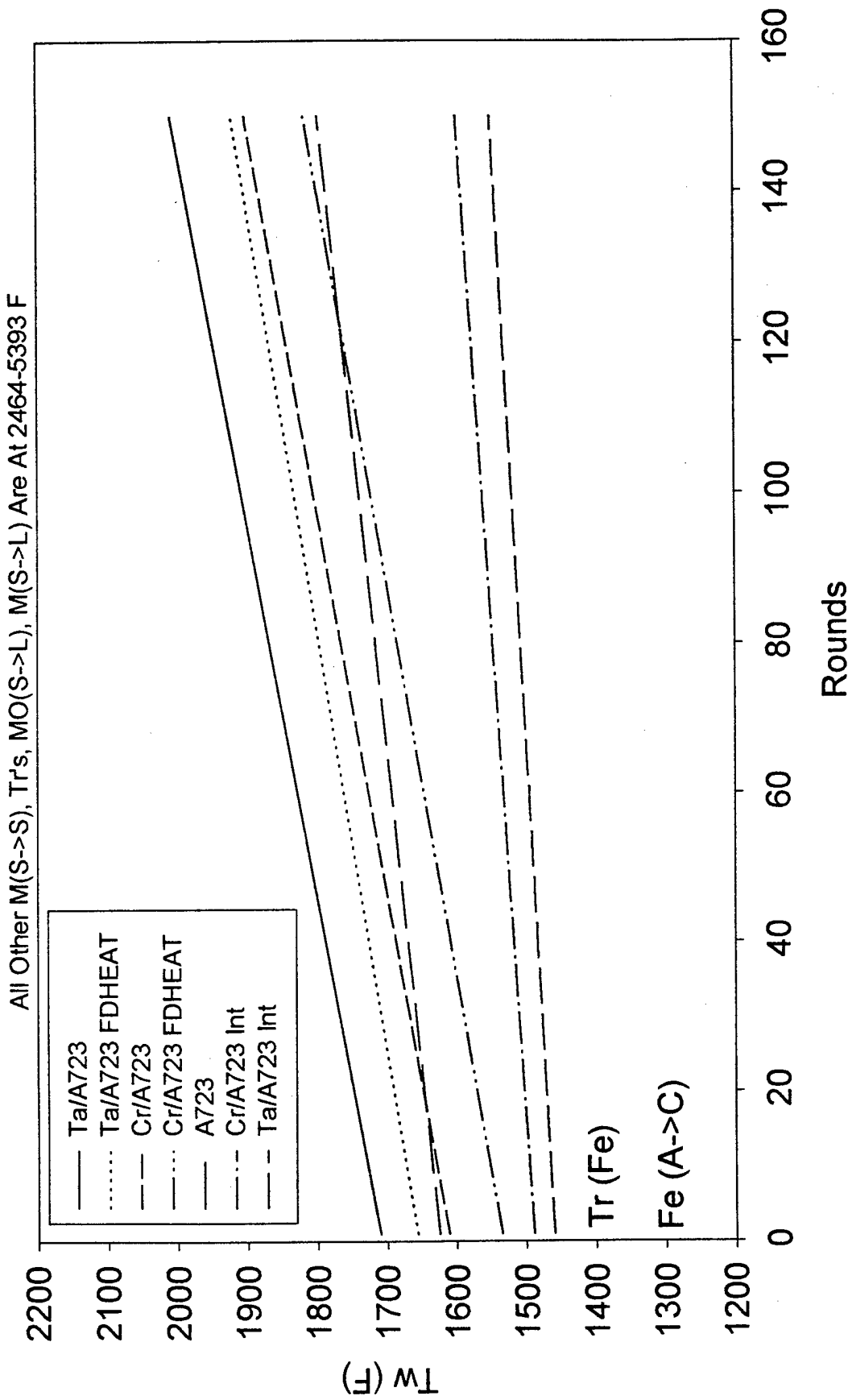


Figure 13 - M919 MACE 30" Maximum Wall Temperatures

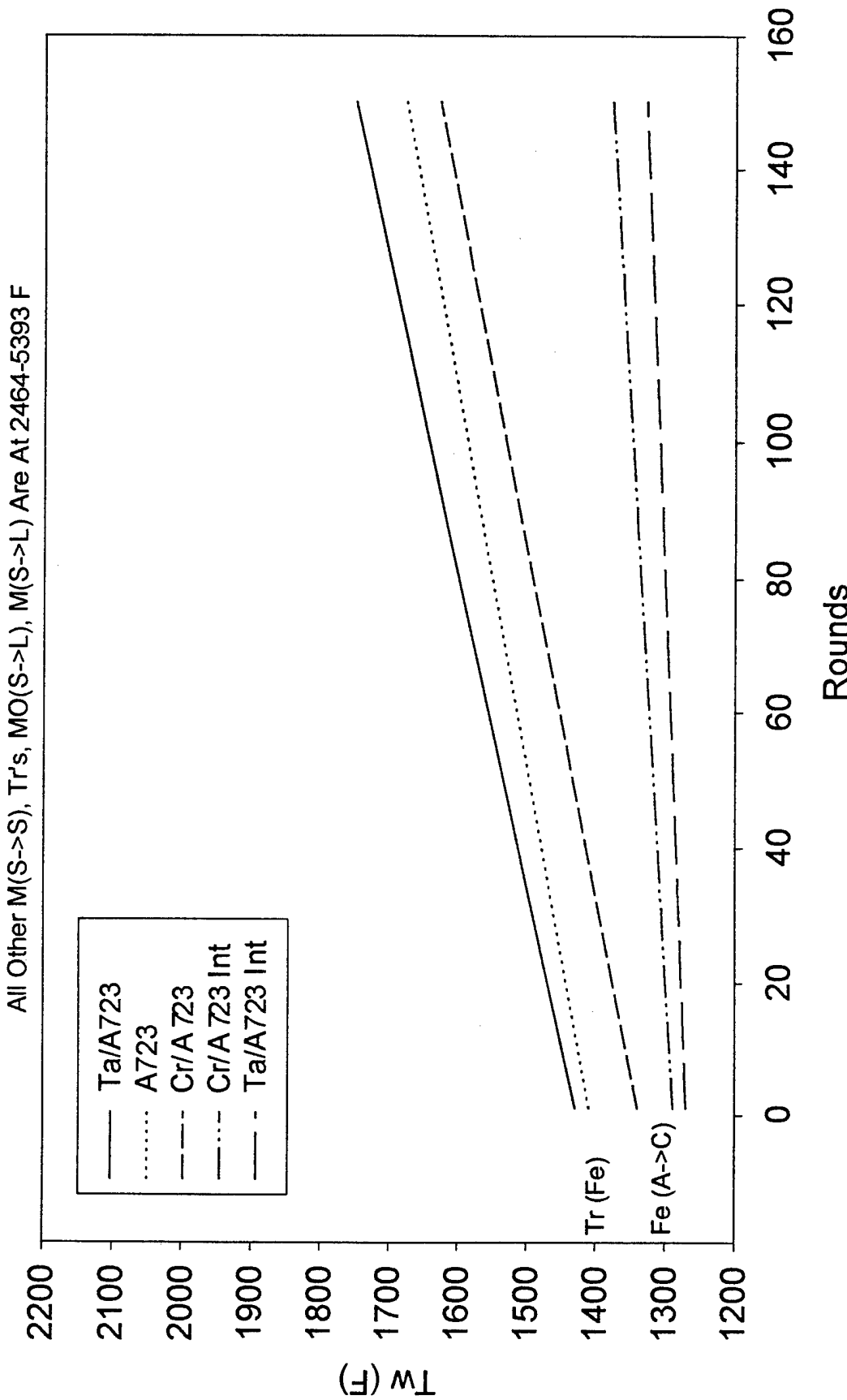


Figure 14 - M919 MACE 6" Cumulative Erosion To Condemnation

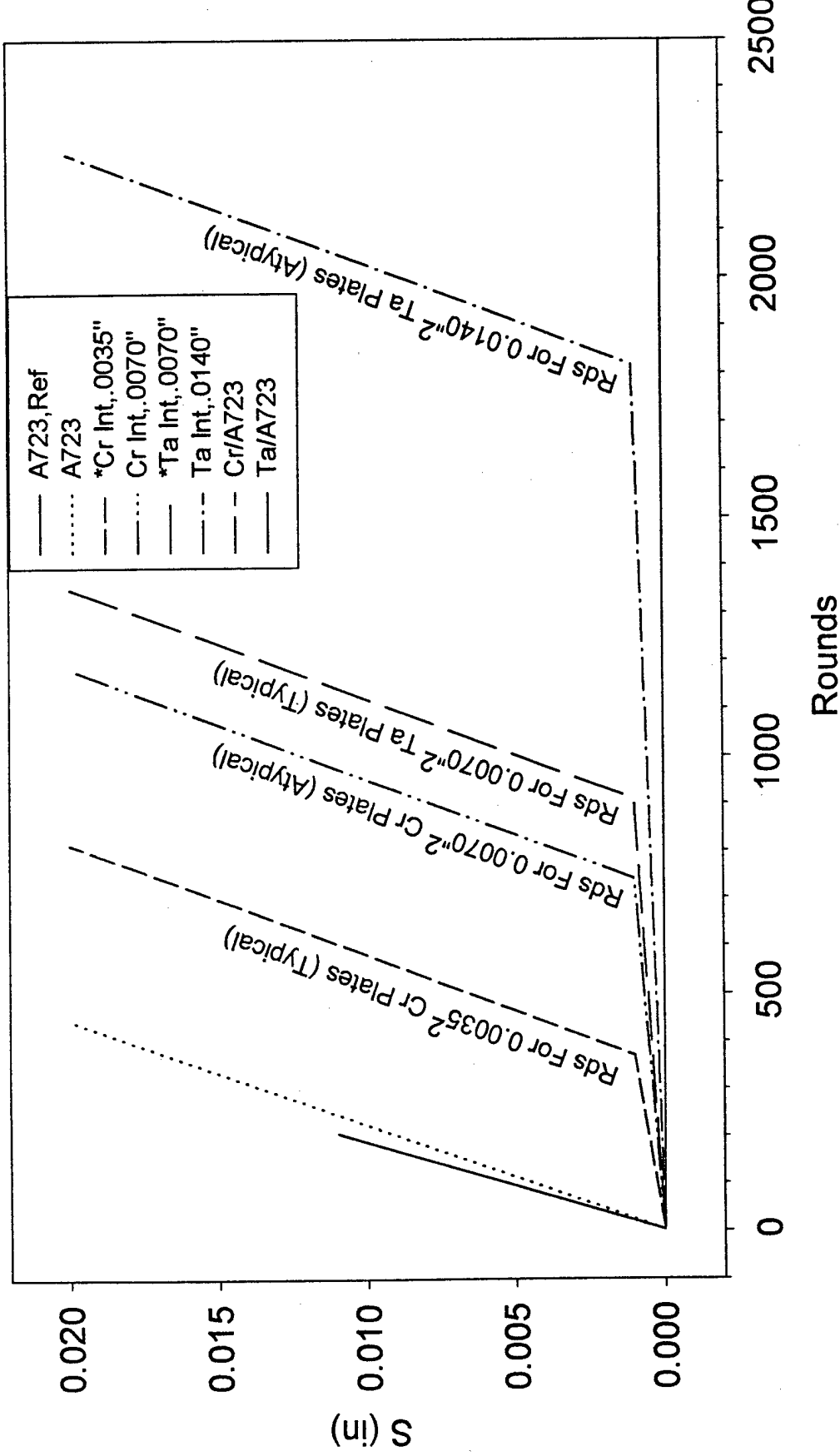


Figure 15 - M919 MACE 12" Cumulative Erosion To Condemnation

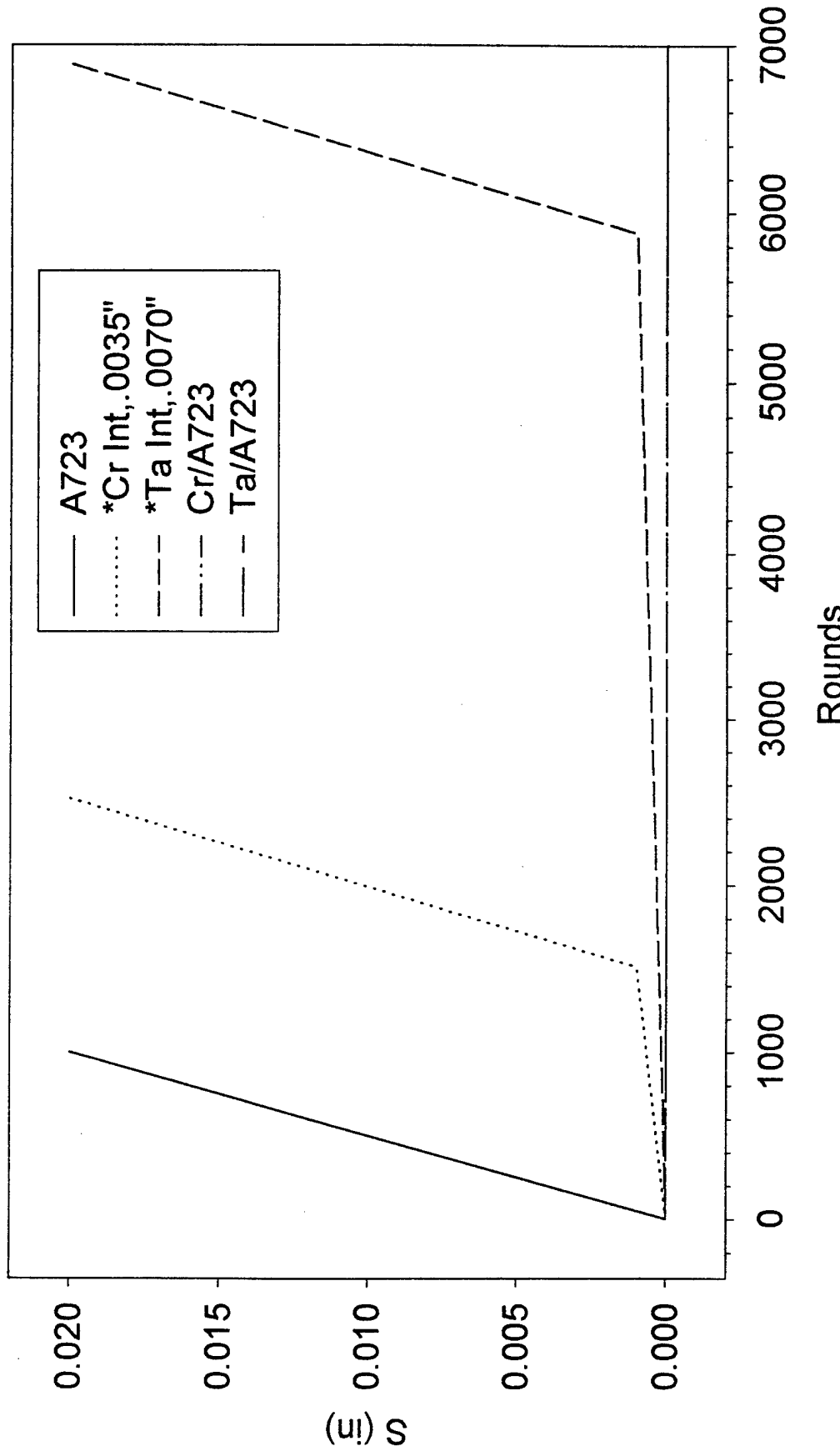
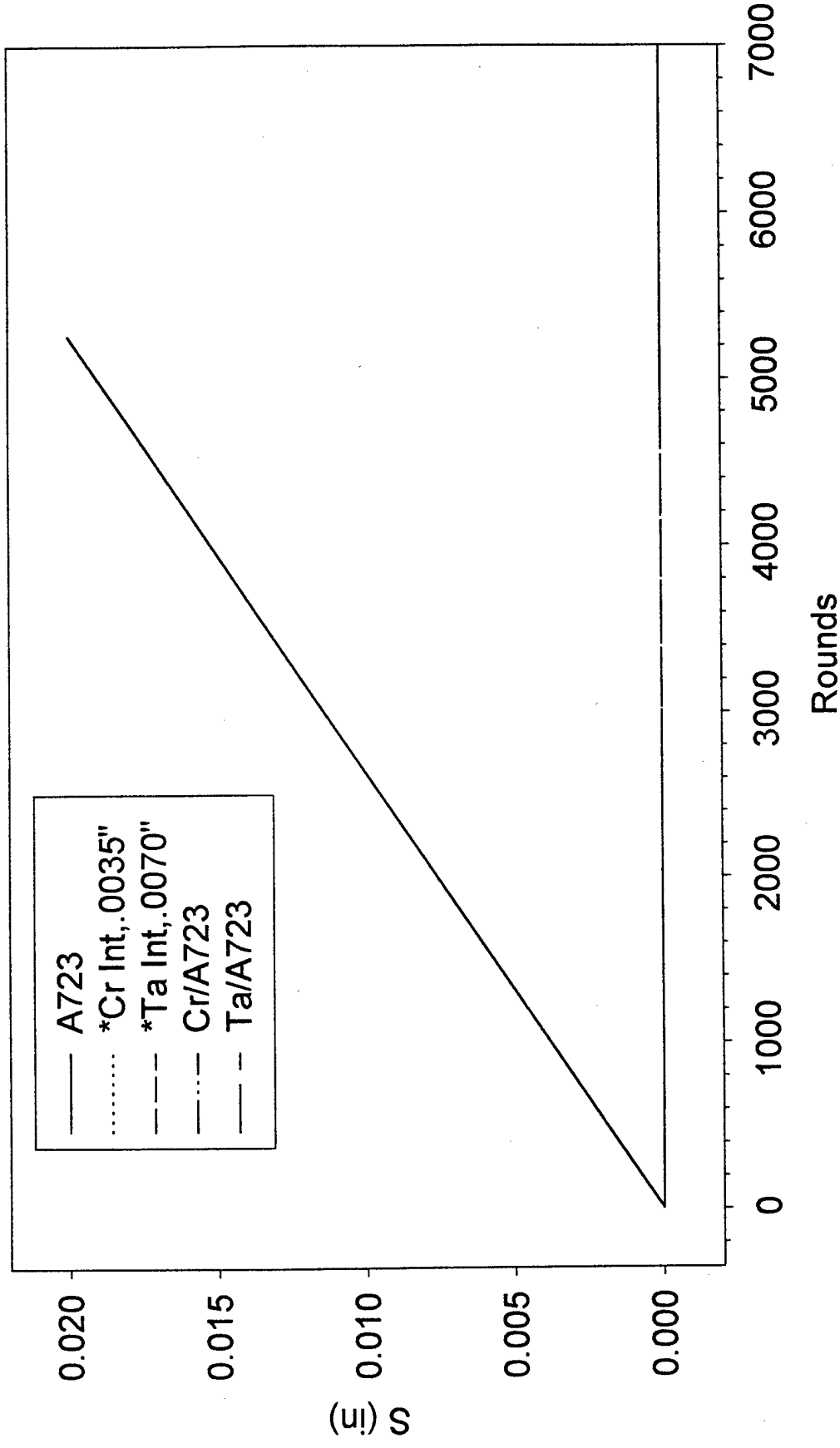


Figure 16 - M919 MACE 30" Cumulative Erosion To Condemnation



TECHNICAL REPORT INTERNAL DISTRIBUTION LIST

	<u>NO. OF COPIES</u>
CHIEF, DEVELOPMENT ENGINEERING DIVISION ATTN: AMSTA-AR-CCB-DA	1
-DB	1
-DC	1
-DD	1
-DE	1
CHIEF, ENGINEERING DIVISION ATTN: AMSTA-AR-CCB-E	1
-EA	1
-EB	1
-EC	1
CHIEF, TECHNOLOGY DIVISION ATTN: AMSTA-AR-CCB-T	2
-TA	1
-TB	1
-TC	1
TECHNICAL LIBRARY ATTN: AMSTA-AR-CCB-O	5
TECHNICAL PUBLICATIONS & EDITING SECTION ATTN: AMSTA-AR-CCB-O	3
OPERATIONS DIRECTORATE ATTN: SIOWV-ODP-P	1
DIRECTOR, PROCUREMENT & CONTRACTING DIRECTORATE ATTN: SIOWV-PP	1
DIRECTOR, PRODUCT ASSURANCE & TEST DIRECTORATE ATTN: SIOWV-QA	1

NOTE: PLEASE NOTIFY DIRECTOR, BENÉT LABORATORIES, ATTN: AMSTA-AR-CCB-O OF ADDRESS CHANGES.

TECHNICAL REPORT EXTERNAL DISTRIBUTION LIST

<u>NO. OF COPIES</u>		<u>NO. OF COPIES</u>		
	ASST SEC OF THE ARMY RESEARCH AND DEVELOPMENT ATTN: DEPT FOR SCI AND TECH THE PENTAGON WASHINGTON, D.C. 20310-0103	1	COMMANDER ROCK ISLAND ARSENAL ATTN: SMCRI-SEM ROCK ISLAND, IL 61299-5001	1
	DEFENSE TECHNICAL INFO CENTER ATTN: DTIC-OCP (ACQUISITIONS) 8725 JOHN J. KINGMAN ROAD STE 0944 FT. BELVOIR, VA 22060-6218	2	MIAC/CINDAS PURDUE UNIVERSITY 2595 YEAGER ROAD WEST LAFAYETTE, IN 47906-1398	1
	COMMANDER U.S. ARMY ARDEC ATTN: AMSTA-AR-AEE, BLDG. 3022 AMSTA-AR-AES, BLDG. 321 AMSTA-AR-AET-O, BLDG. 183 AMSTA-AR-FSA, BLDG. 354 AMSTA-AR-FSM-E AMSTA-AR-FSS-D, BLDG. 94 AMSTA-AR-IMC, BLDG. 59 PICATINNY ARSENAL, NJ 07806-5000	1 1 1 1 1 1 2	COMMANDER U.S. ARMY TANK-AUTMV R&D COMMAND ATTN: AMSTA-DDL (TECH LIBRARY) WARREN, MI 48397-5000	1
	DIRECTOR U.S. ARMY RESEARCH LABORATORY ATTN: AMSRL-DD-T, BLDG. 305 ABERDEEN PROVING GROUND, MD 21005-5066	1	COMMANDER U.S. MILITARY ACADEMY ATTN: DEPARTMENT OF MECHANICS WEST POINT, NY 10966-1792	1
	DIRECTOR U.S. ARMY RESEARCH LABORATORY ATTN: AMSRL-WT-PD (DR. B. BURNS) ABERDEEN PROVING GROUND, MD 21005-5066	1	U.S. ARMY MISSILE COMMAND REDSTONE SCIENTIFIC INFO CENTER ATTN: AMSMI-RD-CS-R/DOCUMENTS BLDG. 4484 REDSTONE ARSENAL, AL 35898-5241	2
	DIRECTOR U.S. MATERIEL SYSTEMS ANALYSIS ACTV ATTN: AMXSY-MP ABERDEEN PROVING GROUND, MD 21005-5071	1	COMMANDER U.S. ARMY FOREIGN SCI & TECH CENTER ATTN: DRXST-SD 220 7TH STREET, N.E. CHARLOTTESVILLE, VA 22901	1
			COMMANDER U.S. ARMY LABCOM, ISA ATTN: SLCIS-IM-TL 2800 POWER MILL ROAD ADELPHI, MD 20783-1145	1

NOTE: PLEASE NOTIFY COMMANDER, ARMAMENT RESEARCH, DEVELOPMENT, AND ENGINEERING CENTER,
BENÉT LABORATORIES, CCAC, U.S. ARMY TANK-AUTOMOTIVE AND ARMAMENTS COMMAND,
AMSTA-AR-CCB-O, WATERVLIET, NY 12189-4050 OF ADDRESS CHANGES.

TECHNICAL REPORT EXTERNAL DISTRIBUTION LIST (CONT'D)

	<u>NO. OF COPIES</u>		<u>NO. OF COPIES</u>
COMMANDER U.S. ARMY RESEARCH OFFICE ATTN: CHIEF, IPO P.O. BOX 12211 RESEARCH TRIANGLE PARK, NC 27709-2211	1	WRIGHT LABORATORY ARMAMENT DIRECTORATE ATTN: WL/MNM EGLIN AFB, FL 32542-6810	1
DIRECTOR U.S. NAVAL RESEARCH LABORATORY ATTN: MATERIALS SCI & TECH DIV WASHINGTON, D.C. 20375	1	WRIGHT LABORATORY ARMAMENT DIRECTORATE ATTN: WL/MNMF EGLIN AFB, FL 32542-6810	1

NOTE: PLEASE NOTIFY COMMANDER, ARMAMENT RESEARCH, DEVELOPMENT, AND ENGINEERING CENTER,
BENET LABORATORIES, CCAC, U.S. ARMY TANK-AUTOMOTIVE AND ARMAMENTS COMMAND,
AMSTA-AR-CCB-O, WATERVLIET, NY 12189-4050 OF ADDRESS CHANGES.
